EFFECTS OF QUENCHING MECHANISM AND TYPE OF QUENCHER ASSOCIATION ON STERN-VOLMER PLOTS IN COMPARTMENTALIZED SYSTEMS

E. BLATT, R. C. CHATELIER, AND W. H. SAWYER
The Russell Grimwade School of Biochemistry, University of Melbourne, Parkville, Victoria 3052, Australia

ABSTRACT Fluorescence quenching techniques have been used extensively in recent years to examine reaction rates and the compartmentalization of components in lipid micelles and membranes. Steady-state fluorescence methods are frequently employed in such studies but the interpretation of the resulting Stern-Volmer plots is often hampered by uncertainties regarding the mode of association of the quencher with the lipid structure and the nature of the quenching mechanism. This paper presents a method for simulating steady-state Stern-Volmer plots in two phase systems, and shows how the forms of such plots are influenced by the type of association of the quencher with the membrane or micelle (partition and/or binding) and by the type of quenching mechanism (dynamic and/or static). Comparisons of simulated plots with experimental data must take into account the possible combinations of quencher association(s) and quenching mechanism(s). The methods presented are applicable to synthetic and natural membranes and provide a basis for comparing the quenching of fluorescent molecules in biological membranes of differing composition.

INTRODUCTION

The quenching of fluorescent molecules has for many years provided useful information on the nature of bimolecular interactions in free solution. In more recent times, the experimental techniques and methods of data analysis have been extended to two-phase systems to study the structural and dynamical properties of molecular assemblies such as detergent micelles and phospholipid bilayers (1). Analysis of the time-resolved and steady-state emission yields information on the permeability of the lipid-water interface to the quencher, the proximity of fluorophore and quencher within the lipid structure and the dynamical properties of the lipid interior.

In most steady-state fluorescence experiments, data is initially presented in the form of Stern-Volmer plots where the quenching efficiency is related to the total quencher concentration (2). In homogeneous solvents of low viscosity, linear Stern-Volmer plots are obtained and the bimolecular rate constant may be calculated from a knowledge of the excited-state lifetime of the fluorophore. Upward-curving Stern-Volmer plots have also been observed as the viscosity of the solvent increases, and can be attributed to a static quenching mechanism (3). Under the latter condition, a fluorophore within a spherical volume surrounding the quencher is quenched instantaneously, while fluorophores located outside an active sphere may be quenched by collisional interactions.

These quenching mechanisms (i.e., dynamic and/or static) have also been proposed to explain the shapes of Stern-Volmer plots in two-phase systems (3–8). However, the nature of the distribution of quencher between aqueous and lipid compartments has not been examined in detail, and the effects of this distribution on the characteristics of Stern-Volmer plots have not been explored. Two distribution processes have been identified: partitioning and binding (9). These are separate thermodynamic processes and cannot be interchanged. The former requires that the ratio of the concentration of quencher between aqueous and lipid phases is constant and independent of the amount of quencher added and of the volume fraction of each phase, whereas the latter implies saturable binding to a limited number of binding sites (10).

Identification of these processes is important from three points of view. First, if values of the bimolecular rate constant for dynamic quenching are to be derived from Stern-Volmer plots, then the abscissa must represent the concentration of quencher in the lipid phase rather than its concentration in the total volume of the system. Second, once the concentration of quencher in the lipid phase is determined experimentally, the data may be tested according to a partition or binding model to distinguish between the two association processes. Finally, the effect of the

E. Blatt's present address is Commonwealth Scientific and Industrial Research Organization, Division of Applied Organic Chemistry, G.P.O. Box 4331, Melbourne, Victoria, 3001, Australia.
R. C. Chatelier's present address is National Institute of Arthritis, Diabetes and Digestive and Kidney Diseases, National Institutes of Health, Bethesda, MD 20205.
Please address all correspondence to W.H. Sawyer.

association process on the form of the Stern-Volmer plot can be considered. This article examines these questions and aims to describe the effects of quenching mechanism and type of quencher association on Stern-Volmer plots for detergent micelles and phospholipid bilayers. Computer-simulated curves highlighting the variety of obtainable shapes are generated for each case, and where appropriate, are used to fit previously published experimental data. The results show that, with careful manipulation of data, comprehensive descriptions of the quenching processes involved are obtainable.

METHOD OF SIMULATING STERN-VOLMER PLOTS

In solvents of low viscosity the quenching efficiency is given by (2)

$$\frac{I_0}{I} - 1 = \frac{\tau_0}{\tau} - 1 = k_q \tau_0 [Q]_T, \tag{1}$$

where I_0, I and τ_0, τ are the fluorescence intensities and lifetimes in the absence and presence of quenchers, respectively, k_q is the bimolecular rate constant and $[Q]_T$ is the total quencher concentration. As the viscosity increases static quenching competes effectively and Eq. 1 becomes (11)

$$\frac{I_0}{I_{exp} W [Q]_T} - 1 = k_q \tau_0 [Q]_T, \tag{2}$$

where W is the static quenching constant. The right-hand side of Eq. 2 vanishes when only static quenching occurs.

For a quencher that associates with a micelle or vesicle, the effective quencher concentration may be given by (12, 13)

$$[Q']_L = \frac{\langle Q \rangle}{V_L}, \tag{3}$$

where $\langle Q \rangle$ is the average number of quenchers per lipid structure and V_L is the molar volume of the lipid structure. $\langle Q \rangle$ can also be expressed in terms of $[Q]_T$ and $[Q]_A$ by (14)

$$\langle Q \rangle = \frac{[Q]_T - [Q]_A}{[M]}, \tag{4}$$

where $[M]$ is the concentration of lipid structures (micelles or bilayer membranes). Substitution of $[Q']_L$ for $[Q]_T$ in Eq. 2 and rearrangement gives

$$\frac{I_0}{I} - 1 = \exp\left(\frac{W\langle Q \rangle}{V_L}\right)\left\{1 + \frac{k_q \tau_0 \langle Q \rangle}{V_L}\right\} - 1. \tag{5}$$

Values of $\langle Q \rangle$ depend on the type of association and can be expressed in terms of a combination of partitioning and binding processes (9, 15)

$$\langle Q \rangle = \langle Q \rangle_p + \langle Q \rangle_b = V_L K_p [Q]_A + \frac{p K_b [Q]_A}{1 + K_b [Q]_A}, \tag{6}$$

where $[Q]_A$ is the concentration of quencher in the aqueous phase, $\langle Q \rangle_p$ and $\langle Q \rangle_b$ are the average number of partitioned and bound quenchers per lipid structure, respectively, K_p is the partition coefficient, K_b is the binding constant, and p is the number of binding sites. A plot of $\langle Q \rangle / [Q]_A$ against $\langle Q \rangle$ is in fact a Scatchard plot from which the type and strength of association may be derived. Determination of the constants K_p, K_b, and p will be discussed in detail in a later section.

Three possible types of association arise: partition, binding, or a combination of partition and binding (9). To simulate Stern-Volmer plots (i.e., $I_0/I - 1$ vs. $[Q]_T$), it is necessary to calculate values of $\langle Q \rangle$ over a range of selected values of $[Q]_T$ and substitute into Eq. 5. This will also allow choice of dynamic and/or static quenching mechanisms.

Partition

In the case of a quencher whose distribution is determined only by a partition equilibrium, $\langle Q \rangle_b = 0$ and the combination of Eqs. 4 and 6 gives $\langle Q \rangle$ in terms of $[Q]_T$

$$\langle Q \rangle = \langle Q \rangle_p = \frac{V_L K_p [Q]_T}{1 + V_L K_p [M]}. \tag{7}$$

At particular values of K_p and $[M]$, the Stern-Volmer plot may be generated by substitution into Eq. 5. The partition coefficient is independent of the volume fraction of each phase and is only limited by the solubility of the quencher in each phase.

Binding

In the case of binding only, $\langle Q \rangle_p = 0$ and the combination of Eqs. 4 and 6 leads to a quadratic of the form

$$A[Q]_A^2 + B[Q]_A + C = 0, \tag{8}$$

where $A = K_b$, $B = pK_b[M] - K_b[Q]_T + 1$, and $C = -[Q]_T$. Solving for $[Q]_A$ at particular values of p, K_b, $[M]$, and $[Q]_T$ allows calculation of $\langle Q \rangle$ and substitution into Eq. 5.

Partition and Binding

In cases where both processes occur simultaneously, a quadratic of the form shown by Eq. 8 is obtained with $A = K_b(1 + K_p V_L [M])$, $B = K_p V_L [M] + pK_b[M] - K_b[Q]_T + 1$, and $C = -[Q]_T$. Substitution of chosen association parameters at various values of $[Q]_T$, and solving for $[Q]_A$, enables calculation of $\langle Q \rangle$ ($= \langle Q \rangle_p + \langle Q \rangle_b$). Since, in effect, there are two populations of quenchers, namely, partitioned and bound, allowance must be made whereby each population can quench fluorescence by static and/or dynamic mechanisms. Under these conditions, Eq. 5 becomes

$$\frac{I_0}{I \exp \dfrac{W(\langle Q \rangle_p + \langle Q \rangle_b)}{V_L}} - 1 = \frac{\tau_0}{V_L}(k_{q,p} \langle Q \rangle_p + k_{q,b} \langle Q \rangle_b), \tag{9}$$

where $k_{q,p}$ and $k_{q,b}$ are the bimolecular rate constants for partitioned and bound quenchers, respectively. Values of $k_{q,p}$ and $k_{q,b}$ may differ (see below). In all fitting procedures, however, we have assumed that both partitioned and bound quenchers have the same static quenching constant.

EXPERIMENTAL METHOD OF DETERMINING ASSOCIATION CONSTANTS

Although a number of standard biochemical techniques exist for determination of association constants, recent developments in steady-state fluorescence quenching methods have provided an alternative procedure in compartmentalized systems. The simplest method of differentiating between binding and partitioning processes is based on a procedure of Encinas and Lissi (15) as extended by Blatt et al. (16). The main assumption is that the quenching efficiency at a particular concentration of quencher is determined by a single independent variable, $\langle Q \rangle$, irrespective of the quenching mechanism or the type of quencher distribution. The concentration of quencher in the lipid phase, $[Q]_L$, with respect

to the total volume of the system is given by

$$[Q]_L = \langle Q \rangle [M]. \quad (10)$$

Making use of the law of conservation of mass

$$[Q]_T = [Q]_L + [Q]_A. \quad (11)$$

Substitution of Eq. 10 into Eq. 11 gives

$$[Q]_T = \langle Q \rangle [M] + [Q]_A. \quad (12)$$

Plots of $[Q]_T$ against $[M]$, at the same quenching efficiency, for a series of values of I_0/I allows determination of $\langle Q \rangle$ as a function of $[Q]_A$. As indicated earlier, the dependence of $\langle Q \rangle/[Q]_A$ on $\langle Q \rangle$ is commonly evaluated in the study of ligand binding to proteins and is known as a Scatchard plot. If only partitioning occurs, a horizontal Scatchard plot is obtained (reflecting the independence of $\langle Q \rangle/[Q]_A$ with $\langle Q \rangle$), and $\langle Q \rangle/[Q]_A$ is directly related to K_p by

$$K_p = \frac{[Q']_L}{[Q']_A} = \frac{\langle Q \rangle}{V_L[Q]_A}, \quad (13)$$

where the primed symbols ($[Q']_L$, $[Q']_A$) refer to concentrations of quencher with respect to the volumes of lipid and aqueous phases, respectively (17). In the case of binding to a single class of independent binding sites, a linear Scatchard plot with a negative slope is obtained and K_b and p are evaluated from the slope and abscissa intercept, respectively (10). When both association processes occur simultaneously, Eq. 6 predicts that $\langle Q \rangle/[Q]_A$ will decrease with increasing $[Q]_A$ (and hence with increasing $\langle Q \rangle$) and will asymptote to a constant value of $V_L K_p$ (15). K_p and p may be calculated from the slope and intercept of the linear region of a plot of $\langle Q \rangle$ against $[Q]_A$ (9) (i.e., when $[Q]_A \gg 1/K_b$). Substitution of these values into a rearranged form of Eq. 6

$$K_b = \frac{\langle Q \rangle/[Q]_A - V_L K_p}{p - [Q]_A(\langle Q \rangle/[Q]_A - V_L K_p)}. \quad (14)$$

The value of K_b may be determined by suitable choice of $\langle Q \rangle$ corresponding to a value of $[Q]_A$.

The association constants obtained from the above analysis can be used to simulate Stern-Volmer plots, as outlined in the previous section. The quenching parameters, k_q and W, are then varied until the best fit of the experimental Stern-Volmer plot is obtained.

COMPARISON OF SIMULATED CURVES WITH EXPERIMENTAL DATA

In this section, Stern-Volmer plots are constructed under differing conditions of quencher association and quenching mechanism and are compared with experimental data obtained in detergent micelles and phospholipid bilayer vesicles. The association parameters chosen for these simulations are those determined previously by experiment.

Partition

An example of partition behavior is seen with dimethylaniline (DMA)[1] as the quencher and Triton X-100 as the lipid structure. The fluorophores used were anthracene, 9-methyl anthracene (9-MA), and *n*-(9-anthroyloxy) fatty acids (n = 2, 6, 9, 12) (16, 18). Horizontal Scatchard plots were found in all cases indicating a partitioning process with no contribution from binding (data not shown). Values of K_p were calculated by substitution into Eq. 13. Stern-Volmer plots were then generated by varying k_q and W in Eq. 5 until best fits were obtained over a range of micelle concentrations. Fig. 1 *a* shows typical experimental data with lines of best fit, and Table I lists the resulting quenching constants obtained for all fluorophores. As expected for quenching in aqueous micellar solutions (5), both quenching mechanisms contribute to the change in fluorescence emission. Also listed in Table I are values of k_q calculated by correcting the abscissa axis of transient Stern-Volmer plots (Fig. 1 *b*) by substitution of $[Q']_L$ for $[Q]_T$ and determination of the slopes of the linear plots. Fig. 1 *b* shows the expected steady-state Stern-Volmer plots (Eq. 1) when only dynamic quenching operates.

Except for 6-AS, excellent agreement between the two extracted values of k_q is obtained (the reason for the unusual behavior of 6-AS is not clear). Although the fluorophores locate at different depths within the lipid structure, little variation in values of k_q is apparent, supporting the notion of micelle homogeneity (17). The microviscosity (19) of the micelle interior may be calcu-

[1] *Abbreviations used in this paper:* 2-AP, 2-(9-anthroyloxy) palmitic acid; *n*-AS, *n*-(9-anthroyloxy) stearic acid (n = 6, 9, 12); 9-MA, 9-methyl anthracene; DMA, N,N-dimethylaniline; SDS, sodiumdodecyl sulphate; CTAB, cetyltrimethylammonium bromide; egg PC, egg phosphatidylcholine.

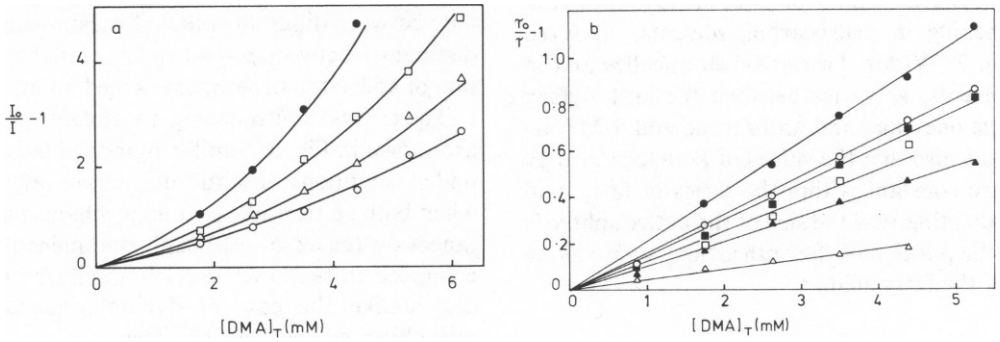

FIGURE 1 Stern-Volmer plots for Triton X-100 with DMA as quencher. (*a*) Steady-state quenching of 9-MA; [Triton X-100] = 0.01 M (●), 0.02 M (□), 0.03 M (△), 0.04 M (○). Lines of best fit were simulated using parameters given in Table I. (*b*) Dynamic quenching in 0.04 M Triton X-100; anthracene (△), 9-MA (□), 12-AS (●), 9-AS (○), 6-AS (■), 2-AP (▲).

TABLE I
PARTITION AND QUENCHING CONSTANTS IN TRITON X-100 WITH DMA AS QUENCHER

Parameter	Fluorophore					
	12-AS	9-AS	6-AS	2-AP	Anthracene	9-MA
K_p	60 ± 2	60 ± 2	60 ± 2	60 ± 2	72 ± 2	64 ± 2
τ_0(ns)	14.0 ± 0.2	13.3 ± 0.2	11.9 ± 0.2	8.7 ± 0.2	3.7 ± 0.2	12.7 ± 0.2
$k_q(10^8\ M^{-1}s^{-1})$*	6 ± 1	5 ± 1	3 ± 1	5 ± 1	4 ± 1	4 ± 1
$k_q(10^8\ M^{-1}s^{-1})$‡	6 ± 1	5 ± 1	6 ± 1	5 ± 1	5 ± 1	4 ± 1
$W(M^{-1})$*	6 ± 0.5	7 ± 0.5	7 ± 0.5	6 ± 0.5	5 ± 0.5	5 ± 0.5
$W(M^{-1})$§	9 ± 0.5	10 ± 0.5	10 ± 0.5	9 ± 0.5	3 ± 0.5	3 ± 0.5

*Best fit from Eq. 5.
‡Calculated from value of K_p and Fig. 1 *b*.
§Values in hydrocarbon solvents taken from Refs. 3 and 18.

lated by substitution of k_q into the modified form of the Debye expression (13).

$$k_q = \frac{8RT}{2000\,\eta}, \tag{15}$$

where η is the microviscosity corresponding to a specific quencher/fluorophore interaction. This results in microviscosities of 16–24 centipoise (cP), compared with previously determined values of between 12–35 cP (12, 20, 21). It has been recognized that the assumptions underlying Eq. 15 are not valid within the confined spaces of micelles and bilayer vesicles (22). Nevertheless, as the above comparison shows, good agreement is observed between this procedure and other fluorescence probe techniques such as fluorescence polarization (20) and changes in quantum yields (21). Values of k_q may also reflect the accessibility of the fluorophore to quencher, as illustrated in protein quenching studies (23, 24).

The static quenching constant, W, has usually been interpreted in terms of an active sphere surrounding the fluorophore. The probability of quenching is 1 if a quencher resides within this sphere of influence. Various combinations of quencher and fluorophore will have different intrinsic values of W and therefore different spheres of influence. Table I summarizes values of W extracted by application of Eq. 5. These are compared with values determined from Stern-Volmer plots of steady-state data for DMA quenching in hydrocarbon solvents, analyzed according to Eq. 2. Within Triton X-100 micelles and in hydrocarbon solvents, W varies between the anthroyloxy fatty acids on the one hand and anthracene and 9-MA on the other. We note also that the values of W determined by both methods are constant within the series of fatty acid fluorophores, indicating that the size of the active sphere is independent of the position of the anthroyloxy group along the acyl chain of the fatty acid.

Binding

Some confusion in the literature exists regarding the descriptive and formal usage of the two association processes, binding and partition. Often, an equilibrium constant is defined either without specifying the type of process (25–28), or expressing the process as binding without adherence to the formal definition of that process (29–31). The latter situation probably arises from the appealing description of ionic quenchers as "binding" to micelles with head-groups of opposite charge. Formal description of the association process as binding, however, requires demonstration that the interaction is saturable and is described by one or more binding constants with their respective site numbers.

To simulate Stern-Volmer plots for the case of binding, we chose to use the thermodynamic (p, K_b) and spectroscopic (k_q, τ_0) parameters pertaining to the quenching of anthracene fluorescence by Cu^{2+} in sodium dodecylsulphate (SDS) micelles (29). The effects of varying K_b and p when only dynamic quenching occurs are shown in Figs. 2 *a* and 2 *b*, respectively. In these plots, $\tau_0 = 5 \times 10^{-9}$ s, and $k_q = 1.2 \times 10^9\ M^{-1}s^{-1}$. (29). An interesting feature of Fig. 2 is the direct proportionality of the quenching efficiency with $\langle Q \rangle$, so that at high concentrations of quencher the curves can be seen to asymptote as $\langle Q \rangle$ approaches p. In Fig. 2 *a*, p is constant ($p = 3$) and K_b is varied between 100 M^{-1} and $K_b \rightarrow \infty$. Here there are significant differences between the curves at low $[Q]_T$, although as $K_b \rightarrow \infty$ ($>10^5\ M^{-1}$) the curves become indistinguishable. Fig. 2 *b* shows that at low $[Q]_T$ it may not be possible to discriminate between different values of p. For example, in order to distinguish between $p = 40$ and $p = 60$, the total concentration of added quencher must exceed 30 mM.

The effects of introducing a static quenching component are shown in Fig. 3. Similar sigmoidal curves are obtained under conditions of static quenching only (curve *a*) and when both static and dynamic mechanisms operate simultaneously (curve *b*), although the quenching efficiency is enhanced in the latter case. It should be noted, however, that unlike the case of dynamic quenching only, the quenching efficiencies, however, are not proportional to $\langle Q \rangle$ and the plateau region will not correspond to a particular value of p.

The simulations shown in Figs. 2 and 3 can now be

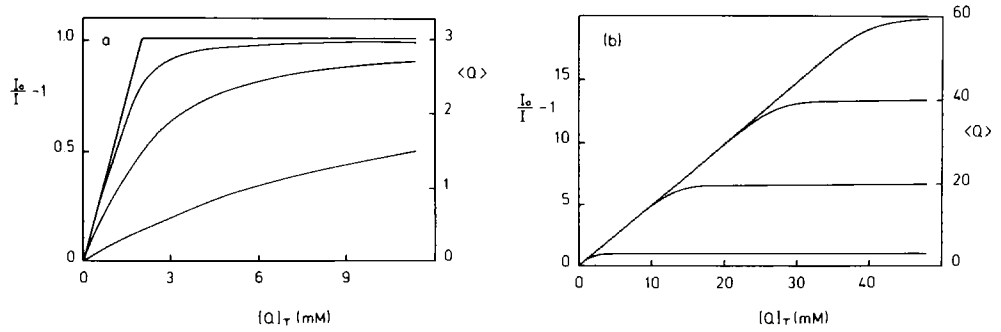

FIGURE 2 Simulated Stern-Volmer plots in the case of binding and dynamic quenching. (*a*) $p = 3$, from *bottom* to *top*, $K_b = 100$, 1,000, 8,800 M^{-1}, and $K_b \rightarrow \infty$. (*b*) $K_b = 8{,}800\ M^{-1}$; from bottom to top, $p = 3$, 20, 40, 60. In both graphs, $\tau_0 = 5 \times 10^{-9}$ s, $k_q = 1.2 \times 10^9\ M^{-1}s^{-1}$ [SDS] = 0.05 M. Note the scale in $\langle Q \rangle$ on the *right* hand side of each figure.

compared with the Stern-Volmer plots of Ziemiecki et al. (Fig. 1 of reference 29). There, the plots curve upward at low $[Q]_T$, but become linear at higher quencher concentrations. Such behavior was attributed to static and dynamic quenching. The quenching data presented, however, could not be reasonably fitted by our model within the following range of values: $W = 0$–$8\ M^{-1}$; $k_q = 0$–$10^{10}\ M^{-1}s^{-1}$ (the upper value of k_q is the diffusion limiting rate constant for water at 20°C); $K_b = 100 - \infty\ M^{-1}$; $p = 1$–60 (the upper value of p is the aggregation number of SDS). Further interpretation and fitting of the data will be presented in the following section.

Partition and Binding

Four combinations are examined in the case of simultaneous quencher partition and binding:

(*a*) dynamic quenching only ($k_{q,p}$, $k_{q,b}$).

(*b*) dynamic quenching for partitioning molecules ($k_{q,p}$) and static quenching for binding molecules (W_b).

(*c*) dynamic and static quenching for partitioning molecules ($k_{q,p}$, W_p) and static quenching for binding molecules (W_b) (i.e., bound quenchers are unable to diffuse).

(*d*) dynamic and static quenching for partitioning and binding molecules ($k_{q,p}$, $k_{q,b}$, W_p, W_b).

Fig. 4 shows typical Stern-Volmer plots according to case *a* where $k_{q,p}$ was constant and $k_{q,b}$ was varied between zero and $k_{q,p}$, that is, we assumed that the translational diffusion of the bound quenchers was less than that for partitioned quenchers. The association constants chosen for the simulations were those obtained for the quenching of 2-AP by 5-nitroxide stearate (5-NS) in egg yolk phosphatidylcholine vesicles (egg PC) (16, 17). In all cases, biphasic plots are observed where the initial slope is due to the contribution of binding and partitioning quenchers and the parallel lines at higher $[Q]_T$ correspond to partitioning quenchers only. An interesting feature of Fig. 4 is the apparent linearity of curve *d* brought about by specific relative values of $k_{q,p}$ and $k_{q,b}$. Such a plot could not be readily distinguished from the case of partitioning with dynamic quenching (see Fig. 1 *b*).

Experimental data for the quenching of 2-AP by 5-NS in egg PC vesicles are plotted in Fig. 5. Clearly, the data do not follow the curvature predicted by case *a* above. However, the points were well fitted by case *d* with quenching parameters of $k_{q,p} = 2.1 \times 10^8\ M^{-1}\ s^{-1}$, $k_{q,b} = 0.7 \times 10^8\ M^{-1}\ s^{-1}$ and $W_p = W_b = 2.8\ M^{-1}$. The significantly higher value of $k_{q,p}$ than $k_{q,b}$ implies that the partitioned quenchers can move more easily from one point in the membrane to another, whereas the bound quenchers are more restricted in their translational diffusion.

Previous quenching studies of anthracene fluorescence

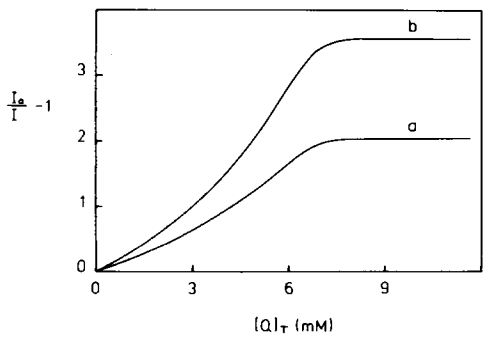

FIGURE 3 Simulated Stern-Volmer plots for binding in the case of (*a*) static quenching only with $W = 2\ M^{-1}$; (*b*) static and dynamic quenching with $W = 2\ M^{-1}$ and $k_q = 1.8 \times 10^8\ M^{-1}S^{-1}$. For both plots, $K_b = 10^5\ M^{-1}$, $p = 10$, $\tau_0 = 5 \times 10^{-9}$s, and [SDS] = 0.05 M.

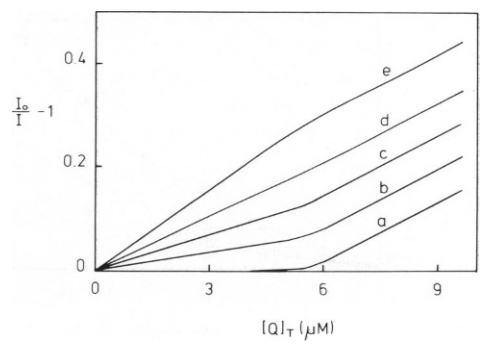

FIGURE 4 Simulated Stern-Volmer plots for the case of binding and partition with dynamic quenching only. Constants chosen were from reference 16 and are $K_p = 3.9 \times 10^4$, $K_b = 10^9\ M^{-1}$, $p = 139$, $\tau_0 = 8.8 \times 10^{-9}$s, [Lipid] = 0.075 mM, $k_{q,p} = 4.5 \times 10^8\ M^{-1}s^{-1}$, $k_{q,b}$ = (*a*) 0, (*b*) 10^8, (*c*) 2×10^8, (*d*) 3×10^8, (*e*) $4.5 \times 10^8\ M^{-1}s^{-1}$.

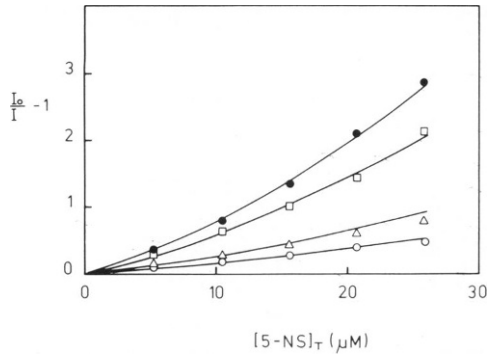

FIGURE 5 Stern-Volmer plots for the quenching of 2-AP by 5-NS in egg phosphatidylcholine vesicles, at [Lipid] = 0.075 mM (●), 0.1 mM (□), 0.2 mM (△), 0.3 mM (○). Association constants were the same as in Fig. 4. Lines of best fit are plotted with $k_{q,p} = 2.1 \times 10^8$ $M^{-1}s^{-1}$, $k_{q,b} = 0.7 \times 10^8$ $M^{-1}s^{-1}$, $W_p = W_b = 2.8$ M^{-1}.

by DMA in cetyltrimethylammonium bromide (CTAB) micelles (15, 32) indicated that the fluorophore locates at the micelle surface. DMA was shown to "bind" specifically to anthracene molecules associated with the micelle, as well as to partition within the lipid phase as revealed by the quenching of fluorophores buried deeper in the micelle (32). Re-examination of the data according to the theory outlined here gave $K_p = 190$, $K_b = 1.23 \times 10^5$ M^{-1} and $p = 1.9$. The experimental points plotted in Fig. 6 are then only fitted well by case *c* with $k_{q,p} = 1.3 \times 10^9$ $M^{-1}s^{-1}$ and $W_p = W_b = 1.6$ M^{-1}. That the bound quenchers do not show a dynamic component is to be expected, since the corresponding DMA/anthracene complexes are tightly held together and will not collide. The value of $k_q = 1.3 \times 10^9$ $M^{-1}s^{-1}$ (corresponding to collisions between partitioned quenchers and anthracene) is approximately three times greater than in Triton X-100 (see Table I), and reflects either easier accessibility of quencher to fluorophore brought about by the concentration of both molecules at the micelle surface, or a lower "viscosity" within CTAB.

A re-evaluation of the quenching data presented by Ziemiecki et al. (29) is now considered. In that study, a binding constant for Cu^{2+} to SDS was determined from the linear region of a Stern-Volmer plot at high values of $[Q]_T$, according to an expression derived by Atik and Singer (33). The model used, however, is applicable to dynamic quenching only. Thus, the linear region was considered to be due to dynamic (or collisional) interactions, and the nonlinear region at low $[Q]_T$ as the result of a static quenching mechanism. This interpretation is unlikely, especially in the case of fluorophores with short excited-state lifetimes (5), and it seems more probable that the two quenching mechanisms contribute simultaneously. (Indeed, as $[Q]_T$ increases the ratio of static quenching to dynamic quenching increases [see Eq. 2]).

We showed earlier that the binding model did not fit the quenching data under a number of different conditions. Plots according to Eq. 12, however, were linear and a Scatchard plot indicated that partitioning (with $K_p \sim 100$) was the main association process. The experimental points were then fitted to the four possible binding and partitioning combinations assuming $K_b = 8{,}800$ M^{-1} and allowing *p* to be an additional variable. Although the best fit was obtained with $p = 3$, it was not possible to distinguish between cases *a*, *b*, or *d*. (Case *c* was clearly inappropriate). Fig. 7 shows the experimental points and typical lines of best fit using case *b*, and Table II lists the parameters obtained for the best-fitted combinations.

It can be seen in Fig. 7 that at [SDS] = 0.05 M and 0.1 M the data are fitted well by the simulated curves, but at [SDS] = 0.15 M there is significant deviation. The reason for this is not clear, although we do point out that in previous studies of quencher association, surfactant concentrations were generally below 0.1 M (25–27, 31–33). There is evidence suggesting changes in micellar shape at high surfactant concentrations (34). Interesting comparisons can be made between the resulting fitted parameters listed in Table II and those obtained by Ziemiecki et al. (29). The case *b* fit gave a bimolecular rate constant corresponding to the partition process of $k_{q,p} = 1.6 \times 10^9$ $M^{-1}s^{-1}$ and a static quenching constant associated with the

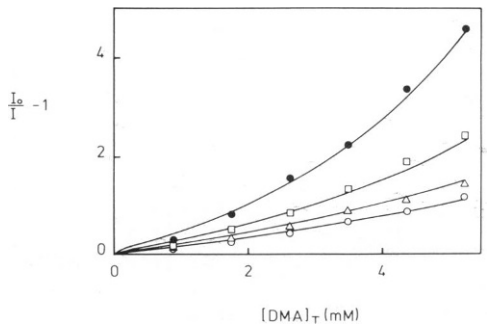

FIGURE 6 Stern-Volmer plots for the quenching of anthracene by DMA in CTAB at [L] = 0.01 M (●), 0.02 (□), 0.03 M (△), 0.04 M (○). Calculated association constants were $K_p = 190$, $K_b = 1.23 \times 10^5$ M^{-1}, and $p = 1.9$. $\tau_0 = 1.22 \times 10^{-9}$ s was taken from reference 32. Lines of best fit are also plotted with $k_{q,p} = 1.3 \times 10^9$ $M^{-1}s^{-1}$, $W_p = W_b = 1.6$ M^{-1}.

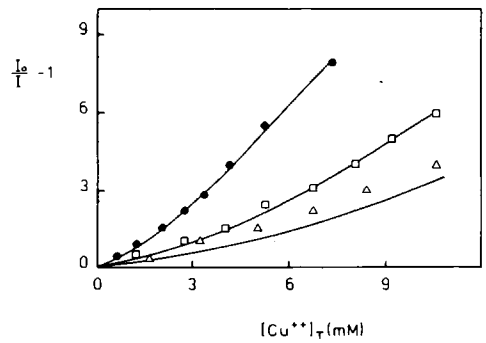

FIGURE 7 Lines of best fit for the fluorescence quenching data of Ziemiecki et al. (29) using case (*b*) binding and partitioning (see text), with $K_p = 100$, $K_b = 8{,}800$ M^{-1} and fitted parameters of $k_{q,p} = 1.6 \times 10^9$ $M^{-1}s^{-1}$, $W = 6.8$ M^{-1}, $p = 3$. [SDS] = 0.05 M (●), 0.1 M (□), 0.15 M (△).

TABLE II
FITTED QUENCHING CONSTANTS FOR THE DATA OF ZIEMIECKI ET AL. (29) FOR THE CASE OF SIMULTANEOUS BINDING AND PARTITIONING*

Parameter	Type of combination		
	(*a*)	(*b*)	(*d*)
$k_{q,p}10^9\ M^{-1}s^{-1}$	5.5 ± 1.0	1.6 ± 0.3	4.6 ± 0.8
$k_{q,b}10^9\ M^{-1}s^{-1}$	1.6 ± 0.3	—	1.7 ± 0.3
$W(M^{-1})$	—	6.8 ± 0.5	0.3 ± 0.1

*Constants were: K_p = 100, K_b = 8,800 M^{-1}, p = 3. Cases (*a*), (*b*) and (*d*); see text.

binding process of W_b = 6.8 M^{-1}. The former value is similar to $k_q = 1.2 \times 10^{-9}\ M^{-1}s^{-1}$ determined from the analysis of lifetime measurements of methylpyrene quenching by Cu^{2+} (27). However, in contrast to the model of Ziemiecki et al. (29), the model presented here is consistent with the nonlinear region resulting from the static quenching mechanism, and the linear region brought about by the dynamic quenching mechanism, that is, once the binding sites are occupied, only the dynamic interactions of the partitioned quenchers and the fluorophore are observed. The value of W is similar to that in Triton X-100 with DMA as quencher (Table I) indicating a radius of active sphere of ~14 Å (35).

The similar dynamic quenching parameters of fits to cases *a* and *d*, and the very low value of W in the latter case, suggest the two combinations cannot be differentiated. Moreover, it seems unlikely that either type describes the experimental results since, as mentioned earlier, a large contribution of static quenching is expected. It should be noted that, in general, case *d* behavior predicts upward curvature as $[Q]_T$ increases (see Fig. 6). Also, the data was well fitted by case *a* due to the small value of p; that is, the linear region at low $[Q]_T$, brought about by dynamic interactions of the binding quenchers, is quickly overshadowed by ensuing partitioning quenchers. This effect can be contrasted to the longer linear regions observed at relatively low $[Q]_T$ when p is much greater (Fig. 4).

It should be noted that the data of Ziemiecki et al. (Fig. 7) is collected under conditions where $[Cu^{++}] \ll [SDS]$ and thus saturation of binding sites is not possible. In such situations where a wide range of fractional saturation of binding sites is not examined, it becomes difficult to determine binding parameters accurately.

Finally, we note that the combination of dynamic quenching with quencher partitioning has been treated by Lakowicz and colleagues (36, 37) in relation to the quenching of carbazole-labeled phospholipids by chlorinated hydrocarbon insecticides. The principle employed, that of using the dependence of quenching on the membrane concentration to determine k_q and k_p, is the same as that discussed here although the method of data analysis is different. In their particular examples it was not necessary to consider the effects of mixed partition-binding associations or of mixed dynamic-static mechanisms.

CONCLUSION

Information about the internal properties of lipid structures and the permeability of lipid/water interfaces to quencher molecules can be obtained by the fluorescence quenching technique. Understanding of the fundamental processes involved, and the effects of compartmentalization on these processes, are requisites for qualitative and quantitative descriptions. This paper has shown the effects of the type of quencher association and quenching mechanism on Stern-Volmer plots in compartmentalized systems, in order to achieve that aim.

The computer simulations and consequent fitting to experimental data, show the variety of situations that can arise from a consideration of the two quenching mechanisms, dynamic and static, and the two association processes, binding and partition.

A particular set of data can sometimes be fitted by a variety of parameters. Under these conditions, however, it is often possible to assess the most likely combination of parameters. The advantage of the fitting procedure is that it enables a comprehensive description of the quenching process from steady-state data alone. Thus, lengthy experiments with expensive equipment (for measuring fluorescence lifetimes) can be circumvented. It should also be noted that in some cases high quencher concentrations are required before various models can be differentiated. Under such conditions, due consideration must be given to the possibility of perturbations in macromolecular structure.

The research was supported by the Australian Research Grants Scheme. Ron Chatelier was the recipient of a Commonwealth Postgraduate Research Award.

Received for publication 11 June 1985 and in final form 20 December 1985.

REFERENCES

1. Fendler, J. H. 1980. Microemulsions, micelles, and vesicles as media for membrane mimetic photochemistry. *J. Phys. Chem.* 84:1485–1491.
2. Stern, V. O., and M. Volmer. 1919. On the quenching-time of fluorescence. *Physik. Zeitschr.* 20:183–188.
3. Blatt, E., K. P. Ghiggino, and W. H. Sawyer. 1981. A novel means of investigating the polarity gradient in the micelle sodium lauryl sulphate using a series of *n*-(9-anthroyloxy) fatty acids as fluorescent probes. *J. Chem. Soc. Faraday Trans.* I. 77:2551–2558.
4. Waka, Y., K. Hamamoto, and N. Mataga. 1978. Pyrene-N,N-dimethylaniline heteroexcimer systems in aqueous micellar solutions. *Chem. Phys. Lett.* 53:242–246.
5. Martens, F. M., and J. W. Verhoeven. 1981. Charge-transfer complexation in micellar solutions. Water permeability of micelles. *J. Phys. Chem.* 85:1773–1777.
6. Eftink, M. R., and C. A. Ghiron. 1976. Fluorescence quenching of indole and model micelle systems. *J. Phys. Chem.* 80:486–493.
7. Wallach, D. F. H., S. P. Verma, E. Weidekamm, and V. Bieri. 1974. Hydrophobic binding sites in bovine serum albumin and erythro-

cyte ghost proteins. Study by spin-labelling, paramagnetic fluorescence quenching and chemical modification. *Biochim. Biophys. Acta.* 356:68–81.

8. Bieri, V. G., and D. F. H. Wallach. 1975. Variations of lipid-protein interactions in erythrocyte ghosts as a function of temperature and pH in physiological and non-physiological ranges. A study using paramagnetic quenching of protein fluorescence by nitroxide lipid analogues. *Biochim. Biophys. Acta.* 406:415–423.
9. Haigh, E. A., K. R. Thulborn, L. W. Nichol, and W. H. Sawyer. 1978. Uptake of *n*-(9-anthroyloxy) fatty acid fluorescent probes into lipid bilayers. *Aust. J. Biol. Sci.* 31:447–457.
10. Klotz, I. M., and D. L. Hunston. 1971. Properties of graphical representations of multiple classes of binding sites. *Biochemistry.* 10:3065–3069.
11. Frank, J. M., and S. J. Wawilow. 1931. Uber die wirkungssphare der ausloschungsvorgange in den fluoreszierenden flussigkeiten. *Z. Physik.* 69:100–110.
12. Costa, S. M. B., and A. L. Macanita. 1980. Transient effects in charge-transfer diffusion-controlled processes in nonionic micelles. *J. Phys. Chem.* 84:2408–2412.
13. Sikaris, K. A., K. R. Thulborn, and W. H. Sawyer. 1981. Resolution of partition coefficients in the transverse plane of the lipid bilayer. *Chem. Phys. Lipids.* 29:23–36.
14. Haigh, E. A., and W. H. Sawyer. 1978. Interpretation of double reciprocal plots used to determine the spectroscopic parameters of bound ligand for binding assays. *Aust. J. Biol. Sci.* 31:1–5.
15. Encinas, M. V., and E. A. Lissi. 1982. Evaluation of partition constants in compartmentalized systems from fluorescence quenching data. *Chem. Phys. Lett.* 91:55–57.
16. Blatt, E., R. C. Chatelier, and W. H. Sawyer. 1984. Partition and binding constants in micelles and vesicles from fluorescence quenching data. *Chem. Phys. Lett.* 108:397–400.
17. Blatt, E., R. C. Chatelier, and W. H. Sawyer. 1984. The transverse location of fluorophores in lipid bilayers and micelles as determined by fluorescence quenching techniques. *Photochem. Photobiol.* 39:477–483.
18. Blatt, E. 1982. Determination of the viscosity and boundary permeability of detergent micelles using fluorescence probe techniques. Ph.D thesis. University of Melbourne. 259 pp.
19. Shinitzky, M., A. C. Dianoux, C. Gitler, and G. Weber. 1971. Microviscosity and order in the hydrocarbon region of micelles and membranes determined with fluorescent probes. *Biochemistry.* 10:2106–2113.
20. Kalyanasundaram, K., and J. K. Thomas. 1977. Micellization, solubilization, and microemulsions. K. L. Mittal, editor. Plenum Publishing Corp., Vol. 2, New York. 569–588.
21. Law, K. Y. 1981. Fluorescence probe for microenvironments: a new probe for micelle solvent parameters and premicellar aggregates. *Photochem. Photobiol.* 33:799–806.
22. Tachiya, M. 1980. Diffusion controlled reactions in a micelle. *Chem. Phys. Lett.* 69:605–607.
23. Eftink, M. R., and C. A. Ghiron. 1976. Exposure of tryptophanyl residues in proteins. Quantitative determination by fluorescence quenching studies. *Biochemistry.* 15:672–680.
24. Eftink, M. R., and C. A. Ghiron. 1977. Exposure of tryptophanyl residues and protein dynamics. *Biochemistry.* 16:5546–5551.
25. Infelta, P. P., M. Gratzel, and J. K. Thomas. 1974. Luminescence decay of hydrophobic molecules solubilized in aqueous micellar systems. A kinetic model. *J. Phys. Chem.* 78:190–195.
26. Almgren, M., F. Griezer, and J. K. Thomas. 1979. Dynamic and static aspects of solubilization of neutral arenes in ionic micellar solutions. *J. Am. Chem. Soc.* 101:278–291.
27. Dederen, J. C., M. Van Der Auweraer, and F. C. De Schryver. 1979. Quenching of 1-methylpyrene by Cu^{2+} in sodium dodecyl sulphate. A more general kinetic model. *Chem. Phys. Lett.* 68:451–454.
28. Dederen, J. C., M. Van Der Auweraer, and F. C. De Schryver. 1981. Fluorescence quenching of solubilized pyrene and pyrene derivatives by metal ions in SDS micelles. *J. Phys. Chem.* 85:1198–1202.
29. Ziemiecki, H. W., R. Holland, and W. R. Cherry. 1980. Solute-micelle binding constants. A simple fluorescence quenching method which is independent of the fluorescence lifetime. *Chem. Phys. Lett.* 73:145–148.
30. Grieser, F., and R. Tausch-Treml. 1980. Quenching of pyrene fluorescence by single and multivalent metal ions in micellar solutions. *J. Am. Chem. Soc.* 102:7258–7264.
31. Grieser, F. 1981. Nitrite quenching of terbium luminescence in sodium dodecyl sulfate solutions. *J. Phys. Chem.* 85:928–932.
32. Blatt, E., K. P. Ghiggino, and W. H. Sawyer. 1982. Fluorescence depolarization studies of n-(9-anthroyloxy) fatty acids in cetyltrimethylammonium bromide micelles. *J. Phys. Chem.* 86:4461–4464.
33. Atik, S. S., and L. A. Singer. 1978. Nitroxyl radical quenching of the pyrene fluorescence in micellar environments. Development of a kinetic model for steady-state and transient experiments. *Chem. Phys. Lett.* 59:519–524.
34. Israelachvili, J. N., D. J. Mitchell, and B. W. Ninham. 1976. Theory of self-assembly of hydrocarbon amphiphiles into micelles and bilayers. *J. Chem. Soc. Faraday Trans.* II. 72:1525–1567.
35. Bowen, E. J., and W. S. Metcalf. 1951. The quenching of anthracene fluorescence. *Proc. R. Soc. A Math. Phys. Sci.* 206:437–447.
36. Lakowicz, J. R., D. Hogen, and G. Omann. 1977. Diffusion and partitioning of a pesticide, lindane, into phosphatidylcholine bilayers. *Biochim. Biophys. Acta.* 471:401–411.
37. Omann, G., and J. R. Lakowicz. 1982. Interactions of chlorinated hydrocarbon insecticides with membranes. *Biochim. Biophys. Acta.* 684:83–95.